



# A novel approach to composite propellant combustion modeling with a new Heterogeneous Quasi One-dimensional (HeQu1-D) framework



S. Varunkumar<sup>a,\*</sup>, M. Zaved<sup>a</sup>, H.S. Mukunda<sup>b</sup>

<sup>a</sup> Department of Mechanical Engineering, Indian Institute of Technology Madras, Chennai 600 036, India

<sup>b</sup> CGPL, Department of Aerospace Engineering, Indian Institute of Science, Bangalore 560 012, India

## ARTICLE INFO

### Article history:

Received 24 June 2016

Revised 18 July 2016

Accepted 26 July 2016

### Keywords:

AP/HTPB composite propellants

Heterogeneity

Serial burning

Extinction

Modeling

## ABSTRACT

This paper is concerned with a new and novel approach to modeling composite propellant burn rate behavior. It is founded on the fact that composite propellant combustion is largely boxed between the premixed limits – of pure AP and fine AP-binder (HTPB, here) whose burn behaviors are taken as known. The current strategy accounts for particle size distribution using the burn time averaging approach. The diffusional effects are accounted for through a calibrated heterogeneous quasi-one-dimensional model (HeQu1-D for short) that allows for the flame temperature dependence on the local AP size-binder thickness geometry. Fine AP-binder homogenization is adopted as in recent models with refinement on the particle size as a function of pressure. The specialty of the present approach is that it invokes local extinction for fuel rich conditions for specific particle sizes when the heat balance causes the surface temperature to drop below the low pressure deflagration limit of AP; this feature allows for the prediction of extinction of propellant combustion. Combining these ideas into a MATLAB<sup>®</sup> calculation framework that uses a single dataset on properties of AP and binder consistent with burn rate vs. pressure of pure AP and fine AP-binder system allows for making the predictions of propellants with multiple particle sizes and different fractions. Comparisons of burn rate data over nearly thirty compositions from different sources appear excellent to good. It is found that it is important to treat the full particle size distribution to achieve better predictions. Low burn rate index ( $\sim 0.25$ ) observed with addition of  $\text{SrCO}_3$  is captured by extending the model to include the effect of binder melt; the gas phase effect is accounted for by calibration against catalytic effect on the fine AP-binder propellant. An interesting deduction from the model is that the temperature sensitivity of propellants should not exceed that of AP. The robustness of the current model and speed of determining the burn rate behavior allow for the possibility of determining the particle size distribution required to meet the burn rate specifications of a specific propellant for practical applications before actually embarking on making the propellant.

© 2016 The Combustion Institute. Published by Elsevier Inc. All rights reserved.

## 1. Introduction

Ammonium Perchlorate-HTPB-Aluminum propellants at high solid loading are the state-of-the-art for space and large defense launch vehicles and equally so, AP-HTPB with little or no Aluminum is the combination adopted in tactical applications to avoid primary smoke. The development of all these propellants has occurred through intuitive reasoning and a number of developmental trials to achieve the specified burn rate behavior. While AP composite propellant model development has been occurring over the last forty years starting with the BDP model (Beckstead-Derr-Price from) with several advances in the details to enhance the under-

standing, rarely are these contemplated as a development tool in practice. The primary reason for this situation is the lack of trust in the model predictions. Cohen [1] has provided a critical view of the strengths and shortcomings of the models and some shortcomings have not been overcome over decades. Some of the propellants required in tactical rocket motors go beyond the simplicity of the composition assumed in the modeling approach. Burn rate indices of 0.25–0.30 are sought along with high energy. Understandably engineering these propellants still relies on empirically determined regression rate variation with pressure ( $p$ ) and initial temperature ( $T_0$ ).

One major approach that takes benefit of the basic BDP model [2], its variant, the petite ensemble model [3] and the modified BDP models [4] is the High Energy Petite Ensemble Model (HYPEM) reported in Blomshield [5]. Predictions obtained for 21 AP/HTPB propellants chosen from [6] by optimizing twelve

\* Corresponding author.

E-mail addresses: [varuns@iitm.ac.in](mailto:varuns@iitm.ac.in), [varunsivakumar@gmail.com](mailto:varunsivakumar@gmail.com) (S. Varunkumar).

### Nomenclature

AP	ammonium perchlorate
HTPB	hydroxy-terminated-polybutadiene
BDP	Beckstead-Derr-Price
$p$	pressure (atm)
$T$	temperature (K)
$O$	initial
HYPEM	High Energy Petite Ensemble Model
$n$	pressure index
$\sigma_p$	temperature sensitivity (%/K)
$\dot{r}$	linear regression rate (mm/s)
$\sigma_p$	temperature sensitivity (%/K)
$\rho$	density (kg/m <sup>3</sup> )
$d_i$	diameter of $i^{\text{th}}$ AP particle ( $\mu\text{m}$ )
$f$	AP mass fraction
$SL$	total AP loading
$pm$	premixed
$bm$	binder-matrix
$ex$	extinction
$t_{bm}$	binder matrix thickness ( $\mu\text{m}$ )
$O/F$	oxidizer-to-fuel ratio
$i$	$i^{\text{th}}$ particle
$l_i$	line average intersection of particle of size $d_i$
$k$	thermal conductivity (W/m-K)
$g$	gas phase
$s$	condensed phase, surface
$f$	flame
$d$	decomposition
$K_r$	average gas phase reaction rate (s/m <sup>2</sup> -atm)
$H$	enthalpy change (kJ/kg)
$x^*$	flame standoff distance ( $\mu\text{m}$ )
$c_p$	specific heat at constant pressure (J/kg-K)
$E$	activation energy (J/mol)
$R$	universal gas constant (8.314 J/mol-K)
$crit$	critical
$eff$	effective
$g_f$	geometric factor
$Z$	non-dimensional AP particle size
$d_0$	diffusion distance ( $\mu\text{m}$ )
$ref$	reference
$f_{ll}$	fraction of particle surface covered by binder melt
$f_{nll}$	fraction of particle surface not covered by binder melt ( $f_{nll} = g_f - f_{ll}$ )
$\xi$	non-dimensional distance, $\xi = \rho_p \dot{r} c_p / k$
SC	strontium carbonate

parameters related to various physical and chemical processes in the condensed and gas phase is shown to result in good comparisons with the experiments for burn rate ( $\dot{r}$ ), index ( $n$ , the exponent in the fit  $\dot{r} = ap^n$ ) and temperature sensitivity ( $\sigma_p$ , the percentage change in  $\dot{r}$  with  $T_0$  at constant pressure) at 1000 psi. The perceptible defect of this model is the lack of attempt to connect these optimized parameters to fundamental physico-chemical processes. This is perhaps the reason why it has not been paid attention to later by other researchers.

The second approach that has been pursued is reactive flow computation of the 3-D propellant packs with detailed and simplified kinetics as a tool for understanding composite propellant combustion process (see [7–13]). The approach is indeed elegant, but the claims of its contribution as a tool for design cannot reach practical propellant engineering groups for two important reasons – the first and more important one is that the physical and chemical effects, like surface behavior with liquid melts cannot be mod-

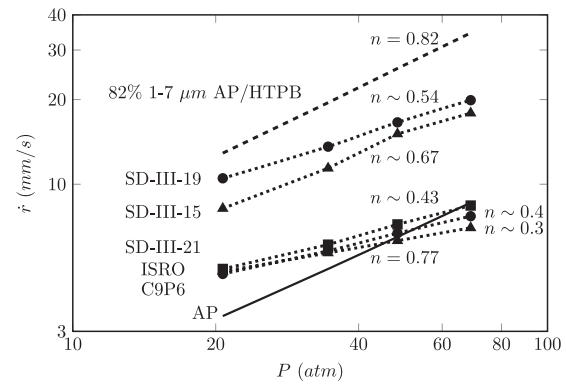


**Fig. 1.** Burn rate and index variation under complete premixed control (AP [17] and 82% 1–7  $\mu\text{m}$  AP/HTPB [4]; influence of lateral diffusion (SD-III-15, 19 and 21 from [6]) and ISRO; effect of additives - LRSAM (SrCO<sub>3</sub>).

eled simply to enable inclusion into the calculations and the second more obvious reason is that the design process is computationally intensive and so time consuming. Further, with the lack of justification for relevance of the complexity of detailed chemistry to predict some overall parameters, it does not seem appropriate that such an effort suggests itself for wider adoption.

In the light of this situation, the present effort is aimed at developing a model that in simplicity must match earlier generation models, but take into account the diffusion process as accurately as promised by the computational strategy. To enable this, the limits of the combustion process – two premixed ends – of the pure AP strand and a strand of very fine AP-binder mix (also with additives) are considered known. A part justification for this approach is that AP itself has been a subject of considerable effort and its physics and chemistry are adequately understood for the present purposes. The burn rate ( $\dot{r}$ ) and temperature sensitivity ( $\sigma_p$ ) variation with pressure as well the low pressure deflagration limits have been captured (see [14,15]) and hence, a simple heat transfer based expression that incorporates the thermodynamic and kinetic parameters (through the transfer number,  $B$  and overall kinetic rate) that gives these output quantities ( $\dot{r}$  and  $\sigma_p$ ) is taken valid. Equally so, the behavior of very fine AP (82% solid loading, 1/7  $\mu\text{m}$ )-HTPB described in Cohen and Strand [4] that is of premixed nature ( $n \sim 0.8$ ) is taken as the highest burn rate achievable (without burn rate modifiers). Lengelle et al. [16] also cites data with 5 micron AP drawn from Cohen [1]. Here again, a simple expression for burn rate with different overall parameters depending on the flame and surface temperatures is taken valid. All propellants with multiple AP particle sizes are taken to burn governed by diffusion related considerations between these limits unless catalytic effects force the burn rate to be much higher or even lower (lower than even AP in some pressure range).

The aspects discussed above are set out in Fig. 1 that shows burn rate data with pressure for several propellants including the limit cases discussed above. The burn rate of SD-III-15, 19 and 21 are drawn from the well documented studies by Miller [6]. The work on AP by Boggs and Zurn [17] has shown that the burn rates and temperature sensitivity ( $\sigma_p$ ) of AP are dependent on the amount of some critical ingredients in it. In particular, Potassium ions (K<sup>+</sup>) that come in due to the production process of AP can affect the burn behavior. This point is considered important because AP affects the burn behavior of the propellant significantly, a feature well known in the literature. A point that will be brought out later concerns  $\sigma_p$  of the propellants; the important result is that the temperature sensitivity of the propellant will be lower than of AP. Thus if low temperature sensitivity of propellants is desired, it is important to ensure that the AP chosen is reasonably pure

and its temperature sensitivity is low ( $\sim 0.2\%/K$ ). The data from Boggs and Zurn [17] shows that  $\sigma_p$  of AP from various sources is anywhere between 0.2 and 1%/K alluding to the presence of impurities. The results of  $\sigma_p$  of a variety of propellants reported in Blomshield [5] are anywhere from 0.17 to 0.32% at 68.9 atm, while that of pure AP is 0.16% [17] at the same pressure. Perhaps the AP chosen in these propellants is "impure". Seeking comparisons on  $\sigma_p$  for propellants with models without the data on  $\sigma_p$  of AP itself may be improper. In the present study, the data on AP chosen is from [17].

While most propellants with a range of sizes of AP burn at a rate higher than that of AP at lower pressure (say, 20 atm, a feature that arises from the additional heat flux from the diffusion flame) they have understandably lower  $n$  that make their burn rate curves intersect the AP line at some pressure. In the region beyond the point of intersection, the combustion process draws away energy from AP rather than enhancing it. This regime has not been investigated by others even though it is of operational importance as some rocket motor combustion instabilities have been ascribed to this behavior (Varunkumar and Mukunda [18]). Most burn rate depressing additives cause this behavior. As can be seen in Fig. 1, SrCO<sub>3</sub> based propellants used in tactical rocket motor having burn rates lower than that of AP beyond 50 atm showed substantial instabilities in the operating pressure range of 70 to 110 atm. Reducing the fraction of this compound significantly and enhancing the burn rate of the propellant closer to that of AP in the operational range of the rocket motor eliminated the instabilities. Part of the motivation for this effort on modeling the steady combustion arose from the investigations on the instabilities.

It is pertinent to point out that the model development presented here benefits from the sequential burning approach suggested by Beckstead [19] and tried out by Lengelle et al. [16] and Kerstein [20] in a limited way; it also adopts the fine particle homogenization idea employed by Gross et al. [12] and Gross [13] with a more appropriate selection of the sizes that allow for homogenization. Further, the present effort accounts for the role of the binder in as important a manner as brought out in experiments of the wide distribution variety by Fredrick Jr [21]. Also, this model goes far beyond in establishing a framework for a much wider class of propellants (with very low burn rate index) and showing their validity for some cases in this paper. The model is termed 'Heterogeneous Quasi One Dimensional model (HeQu1-D)', the word "quasi" being related to the accounting of the two-dimensional diffusional behavior in an equivalent one-dimensional sense.

The rest of paper is organized as follows – (1) HeQu1-D model and theory of local extinction, (2) idea of 'critical pressure', (3) predictions and comparison with experiments, (4) effect of burn rate modifiers and (5) conclusions.

## 2. The HeQu1-D model

The model consists of three parts, namely, (1) multi-modal propellant geometry, (2) 1D deflagration model for pure AP and homogeneous propellant (pseudo- or binder-matrix propellants) and (3) quasi-1-D deflagration model for binder-matrix coated AP particles.

### 2.1. Multi-modal AP propellant geometry

The first step in the development of a serial burning based model for AP/HTPB composite propellants is a geometric description of the multi-modal particle distribution along a random line through a section of the propellant and its statistics. The following sections present aspects related to such a geometric description, namely apportioning of binder matrix and as to what constitutes a statistical path through a propellant.

#### 2.1.1. Apportioning of binder matrix

In general, a multi-modal AP/HTPB propellant consists of AP particles (of density  $\rho_{AP} = 1950 \text{ kg/m}^3$ ) of size  $d_1, d_2, d_3, \dots, d_n$  with corresponding mass fractions  $f_1, f_2, f_3, \dots, f_n$ , such that  $\sum f_i = SL$ , where  $SL$ , is total AP solid loading in the propellant; fuel mass fraction,  $f_{HTPB} = 1 - SL$  and density of HTPB ( $\rho_{HTPB}$ ) is taken as  $975 \text{ kg/m}^3$ . Since combustion of AP particles smaller than a certain size is premixed, these are homogenized with fuel and the resulting HTPB-fine AP mixture is termed 'binder-matrix'. This critical size ( $d_{pm}$ ) is a function of pressure, given by  $d_{pm} = 16 \exp(-0.02p)$  (where  $d_{pm}$  is in  $\mu\text{m}$  and  $p$  in atm) and is deduced from the experimental burn rates reported in [6] for propellants in which the smallest particle size is varied from 0.7 to 20  $\mu\text{m}$  by maintaining the rest of distribution. A similar approach for homogenization is adopted in the work of Gross and others (see [12,13]). In addition to this, a new criterion for homogenization based on extinction of highly fuel rich AP particles is introduced. This is a new feature uncovered by the current model and a detailed description is presented later. Anticipating this, the mass fraction of AP particles incapable of undergoing self-sustained deflagration, denoted  $f_{ex}$ , is also homogenized with the fuel in addition to the fraction determined by the premixed limit criterion. Hence the mass fraction of the binder-matrix is  $f_{bm} = f_{HTPB} + f_{pm} + f_{ex}$ , where  $f_{pm}$  is the mass fraction of AP particles with size smaller than  $d_{pm}$  and  $f_{ex}$  is the mass fraction of quenched AP particles. Then the density of the binder-matrix is given by Eq. (1).

$$\rho_{bm} = \frac{f_{HTPB} + f_{pm} + f_{ex}}{f_{HTPB}/\rho_{HTPB} + (f_{pm} + f_{ex})/\rho_{AP}} \quad (1)$$

The volume fraction corresponding to  $f_{bm}$  (calculated using the binder matrix density,  $\rho_{bm}$ , given in Eq. (1)) is assumed to be distributed over the surface of rest of the AP particles, such that the resulting thickness of binder matrix ( $t_{bm}$ ) is the same for all particle sizes and can be obtained by solving Eq. (2).

$$\frac{f_{HTPB}}{\rho_{HTPB}} + \frac{f_{pm} + f_{ex}}{\rho_{AP}} = \sum_i \frac{f_i [(1 + 2t_{bm}/d_i)^3 - 1]}{\rho_{AP}} \quad (2)$$

Eq. (2) is obtained by equating the volume of the binder-matrix in a propellant (LHS) to the volume occupied by the binder-matrix around all the AP particles (RHS) if it is coated with thickness  $t_{bm}$ . The binder thickness for a given propellant is a value that satisfies Eq. (2). For a single particle size propellant, the equation will reduce to,

$$t_{bm} = \frac{d_{AP}}{3(O/F)}$$

where  $O/F$  is the overall oxidizer-to-fuel ratio ( $f_{AP}/f_{HTPB}$ ) of the propellant; the ratio of density of AP to HTPB is taken to be 2 and that the binder thickness is small compared to the AP particle size. For example, a single particle size of 200  $\mu\text{m}$  80% AP/HTPB propellant will have a binder thickness of 13.3  $\mu\text{m}$  using the approximate formula and 14.5  $\mu\text{m}$  from the exact formula (Eq. (2)), a deviation of 8%. All other reported results are obtained with the exact formula.

One of the important outcomes of this geometric description is the oxidizer-to-fuel ( $O/F$ , ratio of AP fraction to HTPB fraction for a particle of particular size) distribution as a function of the particle size. To calculate ( $O/F$ ) the AP fraction in the binder matrix ( $SL_{bm}$ ) is required in addition to binder-matrix thickness ( $t_{bm}$ ). Fraction of AP in the binder-matrix ( $SL_{bm}$ ) is the ratio of mass fraction of homogenized AP to the sum of the mass fractions of homogenized AP and HTPB as shown in Eq. (3).

$$SL_{bm} = \frac{f_{pm} + f_{ex}}{f_{HTPB} + f_{pm} + f_{ex}} \quad (3)$$

From the binder matrix thickness ( $t_{bm}$  from Eq. (2)), density (Eq. (1)) and solid loading (Eq. (3)), the oxidizer-to-fuel (AP to

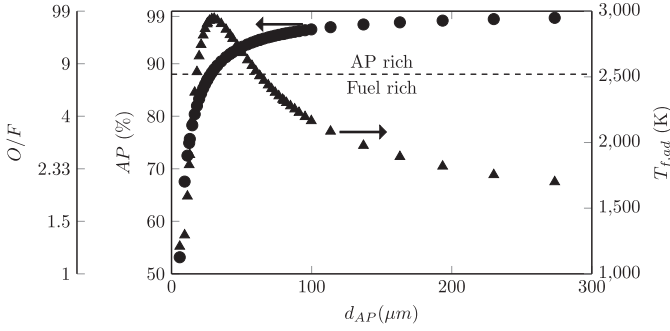


Fig. 2. Variation of particle O/F and adiabatic flame temperature of SD-III-18 [6] at 20.7 atm without extinction).

HTPB) ratio distribution for a particle of particular diameter in a propellant is calculated using Eq. (4).

$$O/F(d_i) = \frac{\rho_{AP} + \rho_{bm} \left[ (1 + 2t_{bm}/d_i)^3 - 1 \right] SL_{bm}}{(1 - SL_{bm}) \rho_{bm} \left[ (1 + 2t_{bm}/d_i)^3 - 1 \right]} \quad (4)$$

where the numerator represents the fraction of AP and the denominator the fraction of HTPB for a binder-matrix coated AP particle.

Adiabatic flame temperature ( $T_{f,ad,i}$ ) of each particle in the propellant is calculated from the O/F distribution using NASA-CEA. Oxidizer-to-fuel ratio and the flame temperature calculated for propellant SD-III-18 (without extinction) from [6] at 20.7 atm are shown in Fig. 2. For convenience,

$$\%AP = \frac{(O/F)}{1 + (O/F)}$$

is also shown. It should be noted that %AP shown here is a function of  $d_i$  and will be used as equivalent of (O/F) in further discussions. The wide variation in the particle (O/F) is a characteristic feature of wide-distribution propellants and accounting for this heterogeneity is shown to be critical to accurate prediction of burn rates and other ballistic properties.

### 2.1.2. Statistical particle path

In the serial burning approach, the propellant regression rate is calculated as the inverse of burning time of a statistically averaged particle path (referred to as just 'line' hereafter) of unit length (see [19]). Such a line consists of an arrangement of binder matrix coated AP particles of various sizes. The fraction of that line composed of a particle of size  $d_i$ , called line average intersection ( $l_i$ ), is proportional to the corresponding volume fraction  $V_i$  [20,22]. To account for the increase in the diameter of each AP particle from  $d_i$  to  $d_i + 2t_{bm}$  due to the binder-matrix coating, the line average intersection is renormalized and calculated for a given propellant using Eq. (5).

$$l_i = \frac{V_i(1 + 2t_{bm}/d_i)}{\sum V_i(1 + 2t_{bm}/d_i)} \quad (5)$$

Figure 3a and b shows a schematic and the statistically averaged particle path calculated for the trimodal propellant SD-III-22 from [6] respectively. Propellant SD-III-22 has binder thickness of 2.3  $\mu\text{m}$  (from Eq. (2)) with 10% AP in the binder-matrix (from Eq. (4)). As can be seen, each nominal particle size (400, 200 and 20  $\mu\text{m}$ ) consists of a wide distribution around the mean size and each particle size contributes significantly to the line average intersection. Given that the O/F variation and hence the individual burn rate is a strong function of the actual particle size, the time contribution from each size distribution must be accurately accounted for while seeking good comparisons with experiments.

The burn time for each binder matrix coated AP particle can be calculated as the ratio of  $l_i$  to the corresponding burn rate ( $\dot{r}_i$ ) and

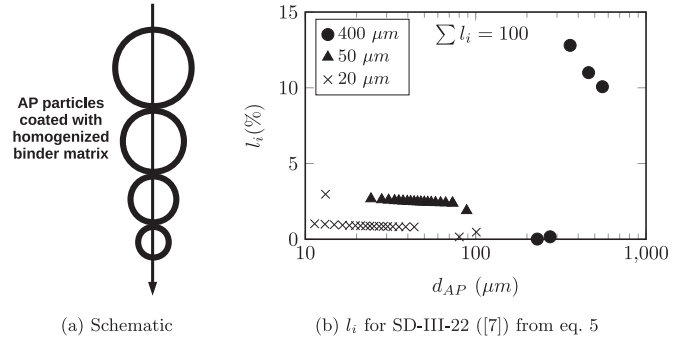


Fig. 3. Statistical particle path.

the burn rate of a propellant ( $\dot{r}$ ) is calculated as the inverse of the total burning time as shown in Eq. (6).

$$\dot{r} = \left[ \sum \frac{l_i}{\dot{r}_i} \right]^{-1} \quad (6)$$

This completes the geometric and the first part of thermo-chemical description of a multi-modal propellant. It remains to calculate  $\dot{r}_i$  to obtain propellant burn rates. Before moving on to the model for predicting the burn rate of individual AP particles coated with binder matrix, a 1-D model for pure AP and binder-matrix will be introduced, with a two fold purpose – first, a method for estimating gas and condensed phase kinetic parameters and their variation using the limiting premixed controlled processes and second, to introduce the idea of 'critical pressure'.

### 2.2. Model for pure AP and homogeneous propellants

Deflagration of pure AP and binder-matrix can be considered 1D with a thin premixed flame transferring heat to the surface of a homogeneous solid. Surface processes are considered to be confined to a thin layer which is taken as an interface between the solid and the gas phases. Heat flux balance at such an interface is as shown in Eq. (7), where LHS is the heat flux into the solid, the first term on RHS is the enthalpy change associated with the phase change process and the second term on the RHS is the heat flux from thin gas phase flame to the surface.

$$k \left[ \frac{dT}{dx} \right]_{0^-} = \rho_p \dot{r} H_s + k \left[ \frac{dT}{dx} \right]_{0^+} \quad (7)$$

where,  $\rho_p$  is the density of the solid,  $\dot{r}$  is the linear regression rate and  $H_s$  is the enthalpy change associated with the phase change at the surface.

The condensed phase is modeled as a homogeneous solid with the temperature profile governed by Eq. (8) along with the boundary conditions. The solution of this equation is given by Eq. (9).

$$\dot{r} \frac{dT}{dx} = \alpha_s \frac{d^2T}{dx^2}; \quad x = 0, T = T_s; \quad x \rightarrow -\infty, T \rightarrow T_0; \quad (8)$$

$$\frac{T - T_0}{T_s - T_0} = \exp\left(\frac{\dot{r}x}{\alpha_s}\right) \quad (9)$$

where,  $\alpha_s$  is the thermal diffusivity of the solid and  $T_s$  is the propellant surface temperature.

Invoking the thin flame approximation, the gas phase is modeled using a 1-D convection-diffusion equation shown in Eq. (10) along with the boundary conditions. The solution is shown in Eq. (11).

$$\rho_p \dot{r} c_p \frac{dT}{dx} = k_g \frac{d^2T}{dx^2}; \quad x = 0, T = T_s; \quad x = x^*, T = T_f; \quad (10)$$

$$\frac{T - T_s}{T_f - T_s} = \exp\left(\frac{\rho_p \dot{r} c_p x^*}{k_g}\right) \quad (11)$$

where,  $k_g$  is the thermal conductivity of the gas phase, assumed constant,  $T_f$  is the gas phase flame temperature and  $x^*$  is the flame standoff distance. Note that these equations are written for a frame of reference translating with the regressing propellant surface assuming constant and equal specific heats ( $c_p = 1150$  J/kg – K).

Flux terms obtained by differentiating the solutions in Eqs. (9) and (11), when substituted in Eq. (7) leads to an expression connecting the regression rate ( $\dot{r}$ ) with flame stand-off distance ( $x^*$ ) and the transfer number as shown in Eq. (12).

$$\frac{\rho_p \dot{r} c_p x^*}{k_g} = \ln\left(1 + \frac{T_f - T_s}{T_s - T_0 - H_s/c_p}\right) \quad (12)$$

Two more conditions are required to close Eq. (12). First is the reactant flux - chemical reaction rate balance for the 1-D premixed flame given by,

$$\rho_p \dot{r} = K_r p^2 x^*$$

assuming second order reaction with  $K_r$  being the average gas phase reaction rate. Substituting the expression for  $x^*$  from Eq. (12) in to this leads to Eq. (13).

$$\rho_p \dot{r} = \sqrt{\frac{k_g}{c_p} K_r p^2 \ln\left(1 + \frac{T_f - T_s}{T_s - T_0 - H_s/c_p}\right)} \quad (13)$$

Arrhenius type pyrolysis law connecting the surface temperature and regression rate,  $\dot{r} = A_s \exp(-E_s/RT_s)$  is the other condition used to close the system. But there are still a few parameter values to be fixed.

### 2.2.1. Choice of physical and chemical parameters

Ingredients of composite solid propellants are complex chemical substances which when subjected to heating undergo transformations involving several steps of physical and chemical processes in solid, liquid and gas phases. To obtain the regression rates of AP and binder matrix from first principles is a task in itself, but not of prime importance to practical propellant model development, given the uncertainties in the parameters associated with each of the subprocesses. In the approach taken here, the process of solid to gas phase change is assumed to be restricted to an infinitely thin interface; reactions in the condensed phase are negligible at pressures of relevance to rocket motor operations (see [23]). Hence the enthalpy change of the physical and chemical processes associated with the phase change enters the surface heat balance equation as jump condition - the first term on right side of Eq. (7). The gas phase combustion process is assumed to be restricted to a thin flame zone at a certain distance away from the interface with a reaction rate quantified by a single parameter  $K_r$  - the resulting temperature profile is an exponential function of distance from the interface (Eq. (11)) and the gas phase heat feedback is given by the second term on the RHS of Eq. (7). In this scenario, the most accurate estimate of the parameters can be obtained by utilizing a combination of the most reliable inputs, namely - (1) measured burn rates of AP, (2) surface pyrolysis kinetic parameters from intrinsic stability constraints, (3) reference surface temperature from low pressure deflagration limit (LPDL) of AP and (4) burn rate of 86% AP binder-matrix. Surface enthalpy change for AP is assumed to be exothermic beyond the LPDL (20 atm); it is very well established that the LPDL is clearly associated with AP surface achieving the melting temperature of around 870 K [14] causing a sudden transition from endothermic sublimation to exothermic decomposition. While the choice of a slight endothermic value in

**Table 1**

Parameter values deduced from deflagration rates of AP and 86% AP binder matrix.

Parameter	Value
AP surface pyrolysis activation temperature, $E_s/R$ (K)	6500 <sup>a</sup>
AP surface temperature at 20 atm, $T_{s,20\text{atm}}$ (K)	870 <sup>b</sup>
Pre-exponential factor for pyrolysis, $A_s$ (mm/s)	5800 <sup>c</sup>
Surface enthalpy change for AP (exothermic), $H_{AP}$ (kJ/kg)	0.6P (atm) + 500 <sup>d</sup>
Surface enthalpy change for HTPB (endothermic), $H_{HTPB}$ (kJ/kg)	-600 <sup>e</sup>
Thermal conductivity, $k_g$ (W/m K)	0.08 <sup>f</sup>
Specific heat, $c_p$ (J/kg K)	1150 <sup>g</sup>
Adiabatic flame temperature of AP, $T_{f,AP}$ (K)	1250 <sup>h</sup>
Adiabatic flame temperature of 86% AP binder matrix, $T_{f,86\%}$ (K)	2850 <sup>i</sup>
Gas phase reaction rate of AP, $K_r, AP$ (s/m <sup>2</sup> atm)	1000 <sup>j</sup>
Gas phase reaction rate of 86% AP binder matrix, $K_r,86\%$ (s/m <sup>2</sup> atm)	30,000 <sup>j</sup>

<sup>a</sup> Intrinsic stability [14].

<sup>b</sup> AP melting temperature, LPDL limit [15].

<sup>c</sup> To satisfy  $\dot{r}_{AP} = 3.3$  mm/s at 20 atm.

<sup>d</sup> From [16].

<sup>e</sup> From [24].

<sup>f</sup> Of air at 1300K.

<sup>g</sup> From [25].

<sup>h</sup> From [16].

<sup>i</sup> Using NASA CEA.

<sup>j</sup> From Eq. (13) with  $\dot{r} = 3.3$  mm/s for AP and 18 mm/s for 86% AP binder matrix [26].

Gross et al. [12] is shown to not influence the predictions significantly (due to the logarithmic dependence, see Eq. (13)), the introduction of the LPDL is essential to capture extinction of highly fuel rich particles. Thermo-physical parameters are taken to be constant and values are chosen at representative temperatures. Surface enthalpy change for HTPB is taken as -600 kJ/kg (endothermic). These choices are well within the limits given in Lengelle et al. [16] for AP and Cohen et al. [24] for HTPB; also the results are not sensitive to the choice due to the slow variation of the logarithm (see Eq. (13)). Thermodynamic equilibrium parameters like adiabatic flame temperatures are calculated using NASA-CEA. Table 1 summarizes the list of parameters, their numerical values and the logic/method used. Note that enthalpy change associated with exothermic process is taken to be positive.

Using the parameters listed in Table 1, predictions obtained are shown in Fig. 4 for deflagration rates of binder-matrix with AP fraction varying from 50–80% at pressures of 6.8, 20.4, 45 and 70 atm.

Two important observations are as follows -

1. Results closely match with the experimental data points obtained from [12], which refers to the original work by Foster et al. [27], indicating the validity of these parameter values.
2. There is a minimum pressure, termed 'critical pressure' ( $p_{crit}$ ), below which the binder matrix ceases to burn as the surface temperature drops below the LPDL value of 870 K. This is obtained from Eq. (13) by using 3.3 mm/s and 870 K for  $\dot{r}$  and  $T_s$  and  $T_f$  and  $K_r$  corresponding to the O/F of the binder matrix. The vertical dashed lines at the left end of each curve indicates this limit in Fig. 4.

This is a new result and to the best of our knowledge, predicted for the first time using a model. Critical pressure values will be used later to classify propellants. The critical pressure values are consistent with the general observation made in [23].

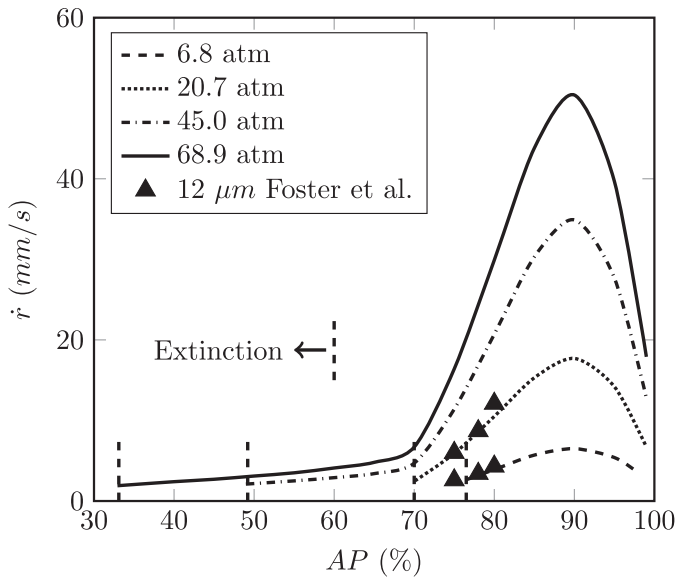


**Fig. 4.** Predicted deflagration rate variation for binder matrix with %AP at different pressures – data points are experimental results of [27] taken from [12]; at pressures values to the left of the vertical dashed lines the compositions cannot undergo self-sustained deflagration (extinction zone).

### 2.3. Quasi-1D deflagration model for binder matrix coated AP particles

In a quasi-1D framework, the burn rate equation for binder matrix coated AP particle retains the same form as that of pure AP and binder matrix (Eq. (13)) with the following modifications –

1. The adiabatic premixed flame temperature,  $T_f$ , is replaced with an effective temperature,  $T_{eff}$  – an analytical model for estimating  $T_{eff}$  is presented later.
2. The premixed gas phase reaction rate,  $K_r$ , is replaced with an effective reaction rate,  $K_{r,eff}$  estimated using an Arrhenius expression obtained by fitting a straight line with two sets of values of  $1/T_f$  and  $\ln(K_r)$  corresponding to that of AP and 86% AP binder matrix. Using the values in Table 1, the following equation is obtained for  $K_{r,eff}$ .

$$K_{r,eff} = 4.3 \times 10^5 e^{-7573/T_{eff}} \quad (14)$$

3. For most practical propellants the AP mass fraction in the binder matrix is too low (<30%) and hence cannot undergo self-sustained deflagration up to very high pressures (>100 atm) – this implies that the gas phase flame directly transfers heat only to a fraction of the total cross section of coated particle excluding the binder matrix. This factor is termed ‘geometric factor’ and is given by,

$$g_f = \left( \frac{d_i}{d_i + 2t_{bm}} \right)^2$$

4. In some model propellants with large fraction of very fine AP particles (< 5  $\mu\text{m}$ ), for example the propellant SD-III-2 in [6], the binder matrix can burn at a rate higher than that of pure AP at corresponding pressure. Such propellants are rarely used in practice.

#### 2.3.1. Extent of lateral diffusion and effective flame temperature

The effective temperature of heat transfer to the particle is dependent on the extent of lateral diffusion of AP and binder decomposition products into each other. The condition for the two limiting cases, namely, AP mono-propellant and premixed binder

matrix limits, is as shown below –

$$d_i \rightarrow \infty \quad T_{eff} \rightarrow T_{f,AP} = 1250 \text{ K}$$

$$d_i \rightarrow 0 \quad T_{eff} \rightarrow T_f = f(O/F)$$

This limiting behavior along with the intermediate cases can be accounted for by Eq. (15), in which the extent of lateral diffusion is quantified by a function of a non-dimensional variable defined as the ratio of AP particle diameter to a diffusion distance ( $d_0$ ).

$$\frac{T_{eff} - 1250}{T_{f,ad} - 1250} = \frac{1 - e^{-Z}}{Z}; \quad Z = \frac{d_{AP}}{d_0} \quad (15)$$

For a finite value of diffusion distance ( $d_0$ ), Eq. (15) captures the two limiting cases shown earlier. The validity of Eq. (15) in the intermediate particle size range is discussed later. The diffusion distance ( $d_0$ ) is limited by the time scale of chemical reaction ( $t_r$ ) between AP and binder matrix decomposition products, that is,

$$d_0 \sim \sqrt{Dt_r} = \sqrt{\frac{\rho_g D}{K_r p^2}}$$

where  $D$  is the diffusion constant,  $\rho_g$  is the gas density,  $K_r$  is the gas phase reaction rate at adiabatic flame temperature corresponding to the particle O/F and  $p$  is pressure in atm. The proportionality constant is accounted for by introducing a reference value for the diffusion distance ( $d_{0,ref}$ ) corresponding to 20 atm pressure and reaction rate of 86% AP loaded particle (30,000  $\text{s/m}^2 \text{ atm}$  from Table 1). Dividing  $d_0$  by  $d_{0,ref}$  and assuming constant  $\rho D$ , an expression as shown in Eq. (16) is obtained for  $d_0$ . The binder matrix thickness is added to the diffusion distance,  $d_0$ .

$$d_0 = d_{0,ref} (1 - \phi) \left( \frac{20}{p} \right) \sqrt{\frac{30,000}{K_r}} + 2t_{bm} \quad (16)$$

With these the three principal modifications listed earlier is accounted for in the burn rate equation and the final form is shown in Eq. (17).

$$\rho_p \dot{r} = \sqrt{\frac{k_g}{c_p} K_{r,eff} p^2} \ln \left( 1 + \frac{T_{eff} - T_s}{T_s - T_0 - H_s/c_p} g_f \right) \quad (17)$$

As stated earlier, the surface enthalpy change ( $H_s$ ) is calculated as mass fraction weighted average of values of AP and HTPB for a particular particle and Eq. (17) is solved simultaneously with the Arrhenius surface pyrolysis law for AP. The functional form for calculating the effective temperature (Eq. (15)) and the choice of reference diffusion distance ( $d_{0,ref}$ ) is such that the burn rates calculated using detailed CFD by Gross and Beckstead [26] for binder matrix coated AP particles of various sizes ranging from 5 to 400  $\mu\text{m}$  is captured. The predicted results, shown in Fig. 5, with  $d_{0,ref} = 90 \mu\text{m}$  match closely with results from [26] for 20.7 and 68.9 atm. This also validates the choice of functional form for calculating effective temperature. A 15% change in the value of  $d_{0,ref}$  led to less than 10% change in the predicted results indicating that the results are not sensitive to the choice of  $d_{0,ref}$ .

With model for all the three components, namely propellant geometry, thermo-physical-kinetic parameters and deflagration rate for binder matrix coated AP particle in place, the following section will present the important phenomenon of extinction.

### 2.4. Phenomenon of extinction

Wide range of AP particle sizes was shown to lead to large variations in oxidizer-to-fuel ratio; one example was shown in Fig. 2 for propellant SD-III-18 [6] at 20.7 atm. Another example, propellant SD-III-22 [6] at 20.7 atm, is shown below in Fig. 6. Fraction of AP (from Eq. (4)) in individual binder-matrix coated AP particles vary from as low a value as 58% for the smallest particle

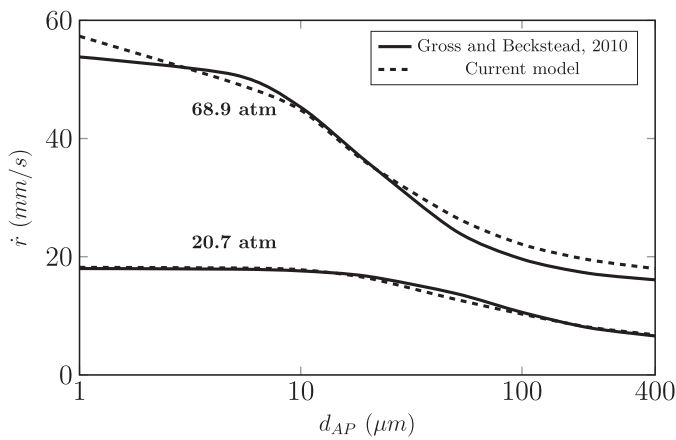


Fig. 5. Comparison of predicted burn rates with  $d_{0,ref} = 90\mu\text{m}$  with CFD results of Gross and Beckstead [26].

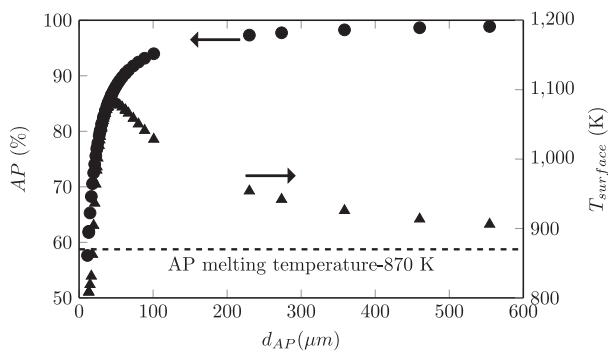


Fig. 6. O/F and surface temperature variation of propellant SD-III-22 at 20.7 atm indicating extinction.

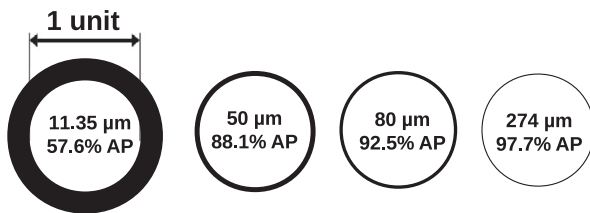


Fig. 7. Cross section of representative particles picked from SD-III-22 at 20.7 atm; the white inner circle represents AP and the black outer coating represents the binder-matrix. All dimensions are scaled by the corresponding particle diameter.

to 99% for the largest. Under such conditions, the predicted surface temperatures (using Eq. (17) and pyrolysis law) for small ( $\leq 25\mu\text{m}$ ) and highly fuel rich particles is less than the LPDL limit of 870 K (see Fig. 6).

Figure 7 shows four representative binder-matrix coated AP particles picked from propellant SD-III-22 for which the O/F and  $T_f$  variation is shown in Fig. 6.

The relative fraction of fuel (proportional to the black area) increases as the AP particle size decreases. Surface heat balance for the  $11.35\mu\text{m}$  particle with an AP fraction of 57.6% results in a surface temperature less than 870 K (LPDL of AP). Same is true for particles up to about  $25\mu\text{m}$  as shown in Fig. 6. Such particles cannot undergo self-sustained deflagration and are considered quenched. This phenomenon of quenching of fuel rich individual particles is termed 'local extinction'. Along with particles small enough to be within the premixed limit at a given pressure, these quenched particles are also homogenized with the binder. Accounting for this is shown later to be critical to obtaining

Table 2  
Summary information of all propellants considered for analysis.

Source	Number	Features
Miller [6] (SD-III-series)	29	High SL – 87.4%; Bi, tri and quad modal; $d_{AP} = 0.7\text{--}400\mu\text{m}$ detailed distribution available
Fredrick Jr [21] (alphabet series)	17	AP – 66.7–87.4%; only mean and $\sigma$ available*
Kumar and Ramakrishna [29] (MIX-I)	1	High SL – 84%; Bi-modal (44–65 and 300–355 $\mu\text{m}$ )
Premiere explosives Ltd. (RD-006 & 007 and C9P6)	3	TCL** AP sieved to a narrow size range RD-006 and RD-007 – 85.65% AP; no additives
HEMRL	1	C9P6 – contains 80% AP and 2.5% $\text{SrCO}_3$ ; distribution available
		Monomodal AP – 69.5%, nominal size of 10 $\mu\text{m}$ distribution available; candidate premixed
		propellant for studying catalyst effects
Kubota [28] K-series	7	Mono- and bi-modal with SL – 65–86% AP only mean particle size available

\* Particle size distribution inferred to be log normal as in Miller [6].

\*\* Tamil Chlorites Limited.

accurate predictions for burn rate variation with pressure (see Section 3.4). In the special case of local extinction of all the particles constituting a propellant, the propellant is considered quenched and the phenomenon is termed 'global extinction'. An example of this would be the propellant C-I reported in [21]. This 66.7%  $16\mu\text{m}$  AP propellant is shown to burn at about 2 mm/s at 17.7 atm but does not undergo self-sustained deflagration at any higher pressures. Capturing this interesting phenomenon with the framework of the current model requires the inclusion binder melt effects and will be not be dealt with here since the focus is on application propellants.

In the following section, predicted steady state results for a number of propellants taken from literature will be presented and discussed. It is important to emphasize that all the following predictions are based on the single set of data set out in Table 1. The extension of the model and additional parameters for the case of burn rate modifiers are discussed separately in Section 4.

### 3. Results

A total of 58 propellants from literature and a few from Indian researchers was chosen for this study. Details of the source and some summary information are set out in Table 2. Based on the consideration that the focus is principally on state-of-the-art compositions with solid loading higher than 82% and that the detailed particle size distribution is critical for ensuring good predictions and hence comparison with experimental data, the following propellants were not considered for analysis – seven from Kubota [28] (adequate particle size information not available), three (A-I, B-I and C-I) from Fredrick Jr [21] (SL < 82%) and one from HEMRL, India (SL < 70%). Also for propellants RD-006 & RD-007 there were uncertainties in measured burn rates associated with the use of ultrasonic water burn method. Measurements from this method has been found to be lower; though issues about the comparisons between the burn rates between this apparatus and a strand burner were not settled adequately, burn rate predictions were obtained (presented and discussed later).

Most commonly the following experimental information reported for AP/HTPB composite solid propellants are:

1. Total fraction of AP in the propellant, also known as solid loading.

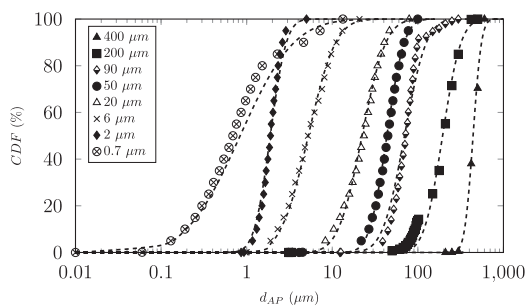


Fig. 8. Detailed particle size distribution of AP used in Miller [6]; data points show the distribution reported in Miller [6]; lines indicate cumulative lognormal distribution computed with the mean and standard deviation of the actual distribution.

2. The nominal particle sizes of AP (weight mean diameter being the most common) that goes into the propellant. Sometimes along with this the standard deviation is also reported.
3. Burn rates at various pressures and in specific studies, at different initial temperatures.

### 3.1. Note on particle size distribution

Of all the sources listed in Table 2, the full particle size distribution is available only in the work of Miller [6]; these are shown in Fig. 8 for all eight nominal sizes used in their work.

It is clear that the distribution is very wide and can be approximated to a good degree of accuracy by a lognormal distribution based on the weight mean diameter and standard deviation. The wide (O/F) distribution for particles constituting a propellant (see Figs. 2 and 6) and that the phenomenon of extinction can be captured only if the full distribution is accounted for in the model calculations implies that reasonable comparisons between model predictions and experiments can be expected only if the detailed distribution or at least the weight mean diameter and standard deviation are available. The source of AP has been indicated in several of the references somewhat indirectly. It was thought that if the manufacturer from which the AP has been sourced is the same and the identified particle size is the same, it is most likely the particle size distribution is also the same. A careful study of the propellant literature was undertaken with the aim of identifying the sources of AP used by investigators in the USA. It became clear by comparison of the distribution given in [30] that the AP used in the studies conducted by Miller [6] and Brewster [31] were sourced from Kerr-Mcgee Chemical Corp. Also by comparison of the mean and standard deviation of AP particle sizes reported in Blomshield and Osborn [32] for the propellants reported in Miller [6] and Fredrick Jr [21] it became clear that AP used is the same and is sourced from Kerr-Mcgee Chemical Corp. Based on these observations, the particle size distribution reported in Miller [6] is used in the model calculations for the propellants chosen from Fredrick Jr [21] for 400 and 20  $\mu\text{m}$  nominal size. For other lots, namely, 9 and 600  $\mu\text{m}$  size AP, a lognormal distribution based on the reported weight mean diameter and standard deviation was used for predictions.

### 3.2. Accuracy and relative errors in experimental results

A clear estimate of accuracy and relative errors in experimental measurement of propellant burn rate is crucial to seeking comparisons with predictions. This information is not available for the 29 propellants from Miller [6] – except for the statement that the measurements were performed in triplicate or duplicate at each pressure. Certain discrepancies are identified in the data based on expectations from the earlier understanding of the effect of AP particle sizes, especially the fraction less than 12  $\mu\text{m}$  at 20.7 atm (the

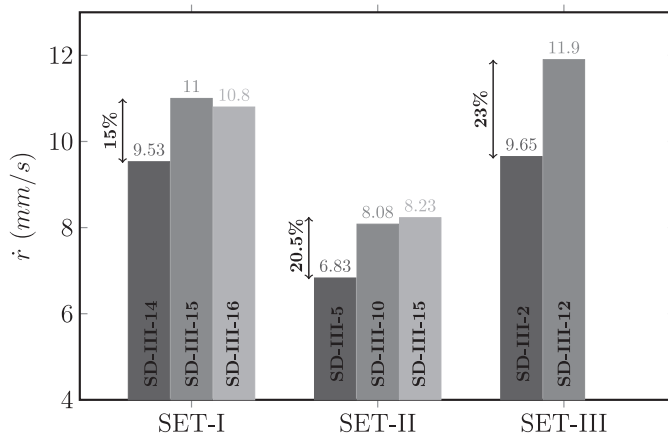


Fig. 9. Inferred accuracy and errors associated with the experimental results of Miller [6].

premixed cut off diameter). This is shown in Fig. 9. For example, propellants SD-III-4, 9 and 14 are composed of same proportion of 400 (48.19%) and 20 (15.66%)  $\mu\text{m}$ , with 0.7, 2 and 6  $\mu\text{m}$  being the rest 36.15% respectively. From the consideration that all 36.15% falls within the premixed cut-off limit at 20.7 atm, the propellant burn rates are expected to be equal. The reported burn rates for SD-III-4, 9, 14 are 9.53, 11.0 and 10.8 mm/s, indicating that variations of 15% magnitude cannot be ruled out (see SET-I in Fig. 9). On similar considerations, comparison of burn rates of SD-III-5, 10 and 15 and SD-III-2 and 12 show an even higher variation of about 21% and 23% respectively (see SET-II and SET-III in Fig. 9). Fredrick Jr [21] has made specific observations about accuracy of experiments including the comparison with propellants made from the same AP source and noted that differences up to 40% is observed at low pressures. At higher pressures though, it is less than 20%. Based on these considerations deviations up to 20% are considered reasonable when seeking comparisons with predictions.

Before presenting results for the burn rate, pressure and temperature sensitivities of these propellants, two crucial ideas need to be introduced – (1) classification of chosen propellant set into two groups based on the critical pressure of the respective binder matrix and (2) effect of local extinction on predicted burn rates.

### 3.3. Classification of propellants based on critical pressure

As stated earlier, for a given AP size distribution, particles below a certain size, determined from the premixed and extinction limits are homogenized with the fuel. This mixture, termed 'binder matrix', is assumed to be coated over the rest of the AP particles with uniform thickness. Dominant controlling processes determining the burning behavior of a propellant varies depending on whether the binder matrix can undergo self-sustained deflagration or not. That is, if the critical pressure ( $P_{crit}$ ) of the binder matrix is lower than the given pressure, then it can undergo self-sustained deflagration and vice-versa. Propellants are classified into two groups (see Table 3) based on the critical pressure of the binder into two groups, namely –

1. *Conventional propellants*, for which  $P_{crit} > P$ ; that is the fraction of AP in the binder matrix is less than the critical value required for self-deflagration. Most practical propellants fall in this category as very rarely is a large fraction of very fine AP used in propellant making – this is related to the fact that the desirable value for the pressure index,  $n$ , is generally less than 0.5 (implying significant diffusion effects).
2. *High fine fraction (HFF) propellants*, for which  $P_{crit} < P$ ; that is the binder matrix can undergo self-sustained deflagration at a

**Table 3**  
Classification of propellant based on critical pressure of binder-matrix based on premixed limit based homogenization.

Propellant type	Prop. ID	Source	
Conventional	SD-III-16 to 26, 28, 30	Miller [6]	
	D-I, E-I, E-I-600A	Fredrick Jr [21]	
	F-I, G-I, G-I-600A		
	H-I, J-I, K-I		
	M-I, N-I, O-I, P-I		
	MIX-I	Ishitha and Ramakrishna [33]	
	RD-007	PEL, Secunderabad	
	High fine fraction (HFF)	SD-III-2 to 6, 8–10, 12	Miller [6]
		SD-III-14-15, 27, 29, 31–33	
		L-I	Fredrick Jr [21]
	RD-006	PEL, Secunderabad	

given pressure  $P$ . Such propellants, shown in Table 3, have an index that is generally greater than 0.6 (indicating premixed dominance) and are rarely used in practice. Propellants which satisfy the condition  $P_{crit} < P$  at least at one value of  $P$  between 20.7 and 68.9 atm are also included in this group.

Model comparisons are presented only for conventional propellants. Though calculations were performed for both types of propellants, comparison with experiments indicate an excellent to good match for conventional propellants and only a reasonable match can be claimed for HFF propellants. This is because the influence of self-sustained deflagration of binder-matrix is not considered at present in the model because HFF propellants rarely find application in actual systems. Before moving on to comparison of predictions with experimental results the important phenomenon of extinction will be discussed.

### 3.4. Effect of local extinction

It was shown earlier that for propellant SD-III-22 at 20.7 atm, particles smaller than  $27 \mu\text{m}$  have a surface temperature less than 870 K and hence cannot undergo self-sustained deflagration. This phenomenon is termed 'extinction' similar to the flammability limits in very rich premixed gas phase fuel-oxidant mixtures. Of course, it is very well known that when strands of propellants are burnt, especially with AP fraction higher than 87.4% as in that of Miller [6], there is no residue left over. This implies that the enthalpy change associated with the gasification of such quenched particles should come from the particles capable of undergoing self-sustained deflagration. This is accounted for in the current model by homogenizing such particles with the fuel. This increases the equivalent binder thickness from 2.3 to  $3.8 \mu\text{m}$  and the % AP in homogenized binder from 10% to 40% for propellant SD-III-22 at 20.7 atm. Propellant burn rates are obtained by solving Eq. (17) for particle surface temperatures by iteratively continuing the calculation till a final solution with minimum surface temperature greater than the LPDL limit of 870 K is achieved. The final O/F and surface temperature variation with particle size for this propellant are shown in Fig. 10. The final predicted burn rate as a function of pressure for SD-III-22 along with the experimental results is shown in Fig. 11a. Predicted burn rates after accounting for extinction show excellent match with the experimental results, including the shift in index between 30–50 atm, compared to the burn rates without extinction.

With the premixed homogenization limit diameter decreasing with pressure, the extinction limit diameter in general decreases with pressure – smaller particles which cannot sustain deflagration at low pressures can do so at high pressures due to increase in the gas phase heat feedback. Figure 11b shows the critical extinction diameter along with the premixed cutoff variation with

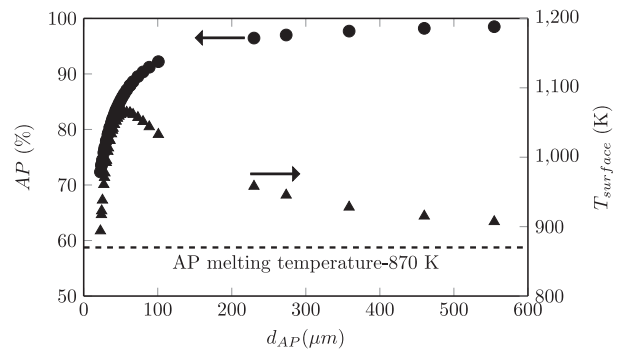
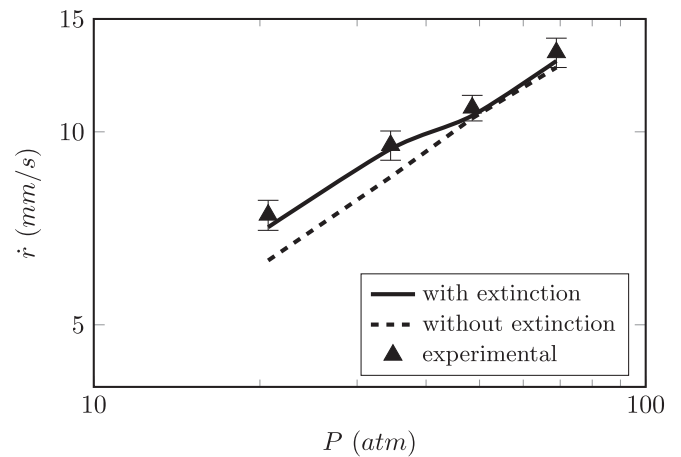
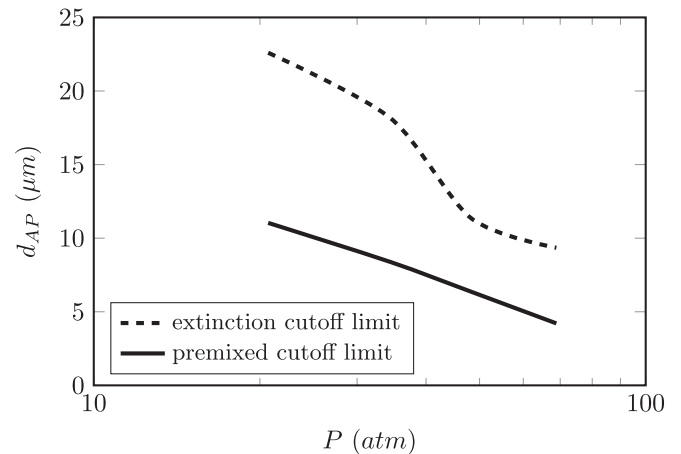


Fig. 10. Calculated O/F and surface temperature for SD-III-22 [6] with extinction.



(a) Experimental vs predicted burn rates without and with extinction



(b) Extinction diameter variation with pressure; premixed cutoff limit shown for reference

Fig. 11. Effect of extinction on model predictions for propellant SD-III-22 from [6].

pressure for propellant SD-III-22 and is consistent with the earlier observation. A very important feature of the prediction accounting for extinction is capture of index change observed in experiments around the pressure range of 30–50 atm. As can be seen, prediction without accounting for extinction fails to exhibit this feature. With further decrease in propellant solid loading the role of extinction will become more significant. In addition to the shift in controlling flame mechanisms with pressure in determining the index, phenomena like plateau and mesa burning can perhaps be explained only by accounting for extinction.

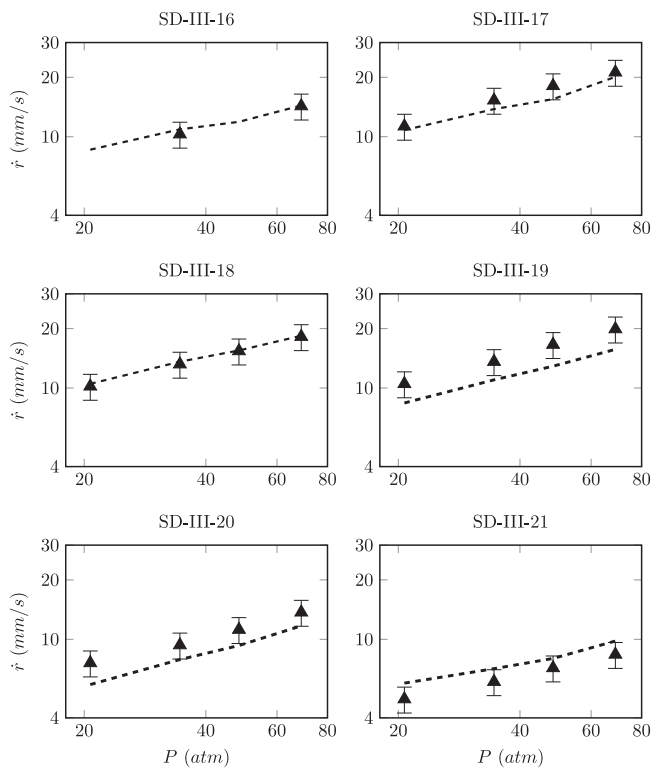


**Fig. 12.** Comparison of predictions with experiments for conventional propellants with %AP  $\geq 86$  from Miller [6].

### 3.5. Burn rate comparison with experiments for conventional propellants

In the following sections detailed comparison of predictions with experimental results will be presented for *conventional propellants*, that is with multi-modal (bi-, tri-, etc.), wide distribution and high SL (%AP  $\geq 84$ ); as stated earlier, most state-of-art practical propellants belong to this category. **Figures 12–16** show the predicted burn rates for the conventional propellants, along with experimental results and the percentage deviation. Predicted burn rates are in excellent agreement with experiments for 14 out of 27 high SL ( $\geq 84\%$  AP). Another 11 are considered good to reasonable, making the tally 25 out of 27 propellants as being reasonable or better. Predictions Mix-I are excellent but for RD-007 are higher than the experimental results by more than 20% even though the AP source is the same and the compositions also nearly same (coarse to fine ratio of 55:45 for RD-007 and 50:50 for Mix-I). The measurement technique for Mix-I is strand burner, but ultrasonics tracked under water combustion for RD-007. For small strands, the heat loss effect can bring down the burn rate and so it is expected that the comparison is indeed satisfactory for this propellant as well. The only high SL propellant with poor prediction is D-I taken from Fredrick Jr [21]. The observed deviation is specific to propellants chosen from Fredrick Jr [21] and in particular for propellants in which the fraction of 16  $\mu\text{m}$  AP particles is very high ( $\geq 64\%$ ) and hence have a significant influence on the burning rate. The likely cause for the deviation is speculated to be due to a significant difference between the reported and the actual particle size distribution of the 16  $\mu\text{m}$  AP in [21]

#### 3.5.1. Temperature sensitivity

Temperature sensitivity ( $\sigma_p$ ), which quantifies the burn rate variation with propellant initial temperature ( $T_0$ ) at constant pressure is another important steady state parameter in addition to

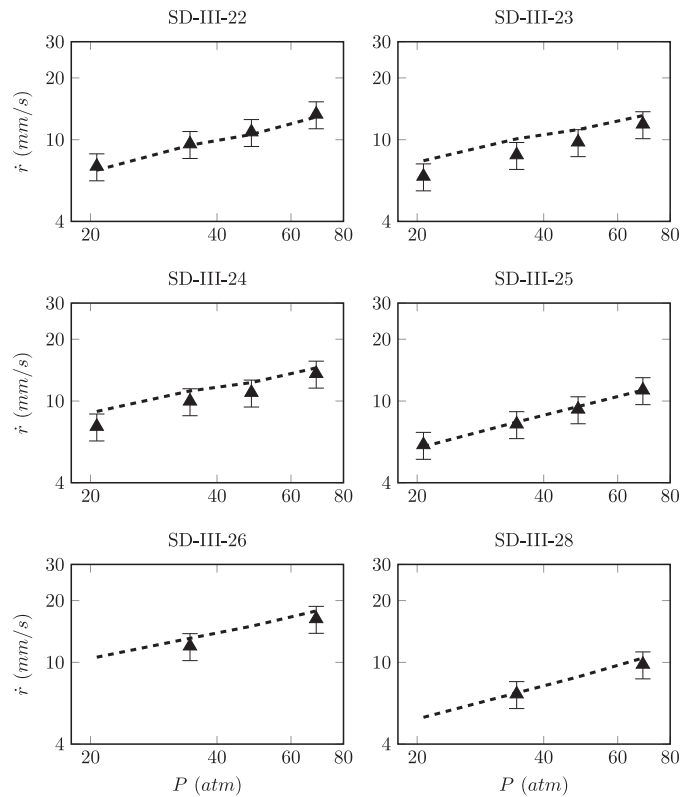


**Fig. 13.** Comparison of predictions with experiments for conventional propellants with %AP  $\geq 86$  from Miller [6].

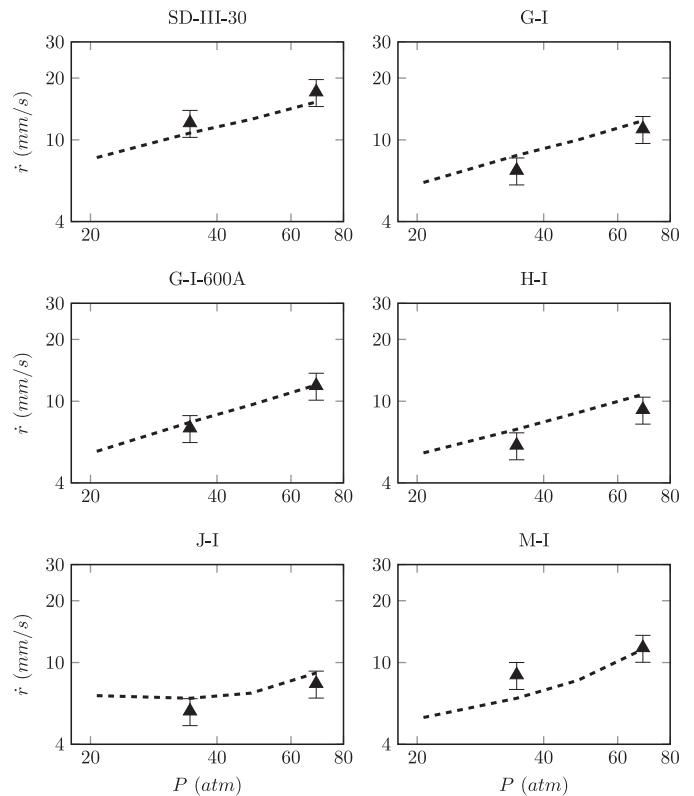


**Fig. 14.** Comparison of predictions with experiments for conventional propellants with %AP  $\geq 86$  from Miller [6], Fredrick Jr [21].

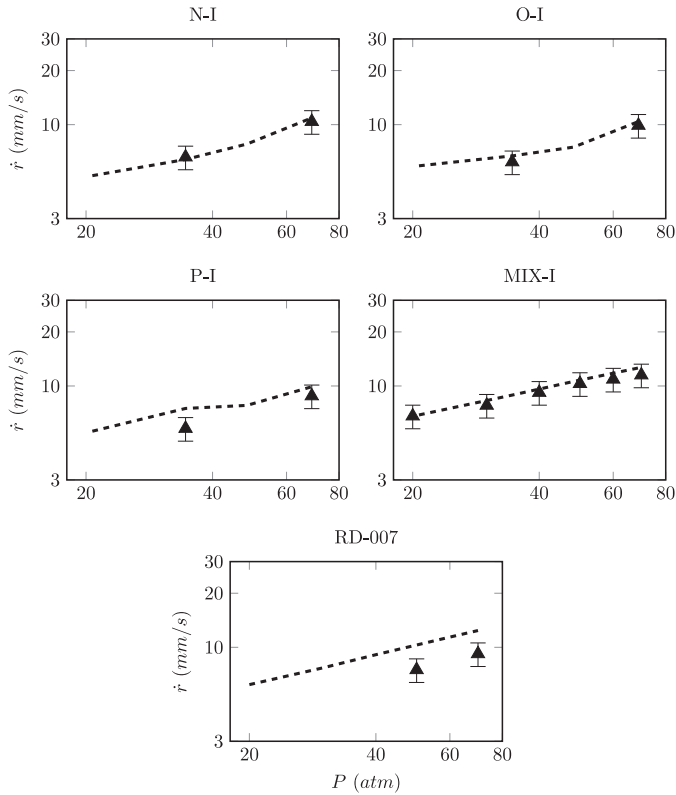


**Fig. 15.** Comparison of predictions with experiments for conventional propellants with %AP  $\geq 86$  from Fredrick Jr [21], Ishitha and Ramakrishna [33] and PEL (see Table 2).

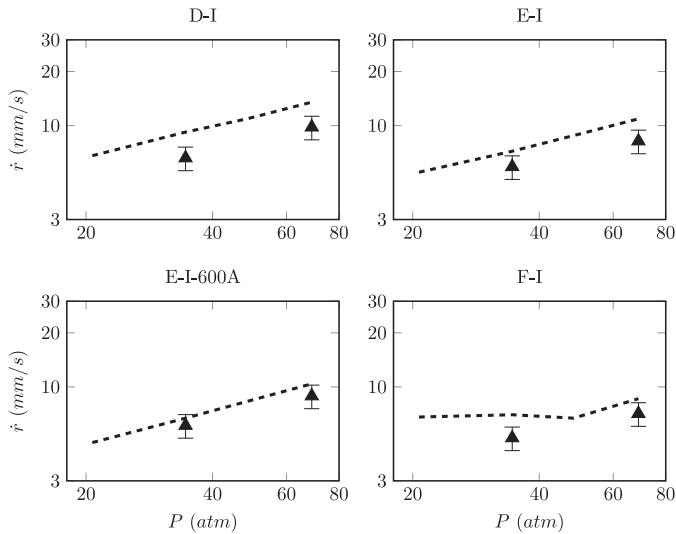


**Fig. 16.** Comparison of predictions with experiments for conventional propellants with %AP = 84 from Fredrick Jr [21].

pressure index. A general closed form expression for temperature sensitivity of a binder-matrix coated AP particle obtained by differentiation of Eq. (17) with respect to  $T_0$  and using the surface pyrolysis law is given by Eq. (18).

$$\sigma_p = \frac{\partial \ln \dot{r}}{\partial T_0} = \frac{B}{2(T_s - T_0 - H_s/c_p)(1+B)\ln(1+B) + \frac{RT_s^2}{E_s}(g_f + B)} \quad (18)$$

The effect of variation of the gas phase flame temperature and hence the reaction rate with initial propellant temperature is negligible compared to the other effects and is ignored. Using this expression and the parameters given in Table 1, the temperature sensitivity for pure AP is calculated to be 0.2%/K at 20.7 atm and 0.15%/K at 68.9 atm. These values match well with the experimental results of Boggs et al. [34]. Similarly the temperature sensitivity of a 86% loaded fine AP/HTPB propellant is predicted to be 0.05%/K at 20.7 atm and 0.03%/K at 68.9 atm. From Eq. (18) it can be concluded that the temperature sensitivity for practical propellants will always decrease with addition of HTPB to pure AP – this is due to the dominant effect of the  $(T_s - T_0 - H_s/c_p)$  term in the denominator of Eq. (18). Also the temperature sensitivity of practical propellant will fall between that of pure AP and premixed AP/HTPB propellants, the two premixed limits. Even for fuel rich AP particles, which can have a surface temperature less than that of AP, but more than  $\geq 870$  K at pressures higher than the LPDL, the effect of endothermicity dominates and decreases the temperature sensitivity from that of AP at corresponding pressure. This is an important general result – the temperature sensitivity of a AP/HTPB propellant can be expected to be always less than that of AP at corresponding pressure. This is consistent with the earlier observations of Cohen and Flanigan [35].

Predicted temperature sensitivity results for conventional propellants fall in the range of 0.06–0.1% K. The temperature sensitivity of a propellant is closely linked to that of the AP used in the processing, which itself is known to increase significantly with addition of impurities like potassium etc., [17] a subject discussed earlier. Since for the current set of propellants chosen from the literature, the sensitivity of AP used in making propellants is not reported, the model is calibrated with the sensitivity values for pure AP reported in [34]. This explains the deviation observed between the predicted values and the experimental results reported in [32].

### 3.6. Space of possible steady ballistic properties

The principal problem confronting propellant designers is that of arriving at a choice for the fraction and distribution of AP particles to achieve a particular ballistic property set – burn rate ( $\dot{r}$ ), pressure index ( $n$ ), and temperature sensitivity ( $\sigma_p$ ). Commercially available AP comes in certain standard nominal sizes and in general with lognormal distributions. Given this, the HeQu1-D model can be used to quickly generate a space of possible burn rates, indexes and temperature sensitivities that can be achieved with the given nominal sizes and distribution with principal variables being the total AP fraction and the relative proportion of each nominal size. A bar graph showing this for three nominal sizes (400, 200, 20  $\mu\text{m}$ ) taken from [6] is presented in Figs. 17–19. These plots show calculated burn rates, index and temperature sensitivity at 68.9 atm for three different fractions of 20  $\mu\text{m}$  AP (15.66, 32.5 and 51.81%) and by varying the relative proportion of 400 and 50  $\mu\text{m}$  for each value of fraction of 20  $\mu\text{m}$  (shown in bottom and top horizontal axis respectively).

At a fixed fraction of 20  $\mu\text{m}$  AP, the burn rate increases with substitution of 50  $\mu\text{m}$  AP particles for 400  $\mu\text{m}$ , consistent with the expectation that burn rate increases with decrease in mean AP particle size at fixed SL. The index, on the other hand, decreases indicating a shift in controlling mechanism from AP mono-propellant flame to diffusion as the fraction of 5  $\mu\text{m}$  increases. At each fixed proportion of 400 and 50  $\mu\text{m}$  AP, decrease in 20  $\mu\text{m}$  AP fraction decreases the burn rate. This effect is more pronounced at higher fractions of 400  $\mu\text{m}$ . The index variation shows an interesting behavior. At high fraction of 400  $\mu\text{m}$  AP (>60%) decrease in fraction of 20  $\mu\text{m}$  AP leads to an increase in index indicating the increased role of AP mono-propellant flame of the 400  $\mu\text{m}$  particles. But this tendency is reversed as the 400  $\mu\text{m}$  AP fraction is de-

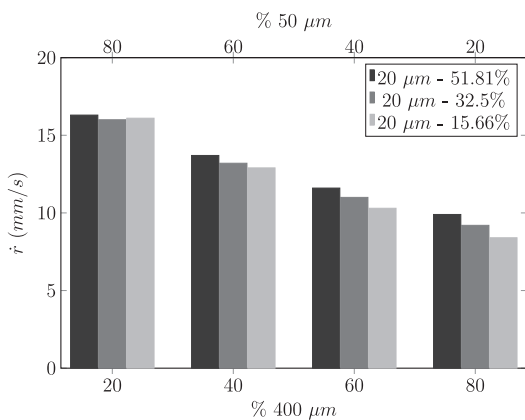


Fig. 17. Space of possible burn rates for 87.4% SL propellant with three nominal AP particle sizes – 400, 50, 20  $\mu\text{m}$  at 68.9 atm.

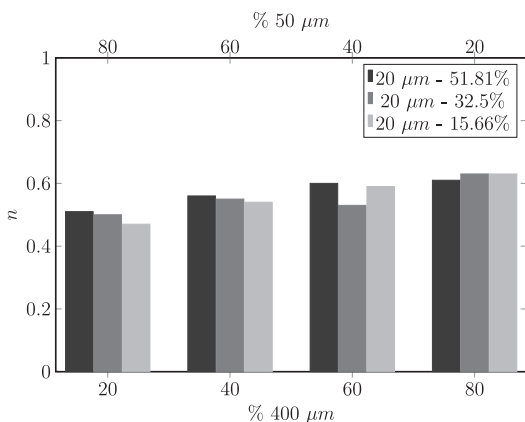


Fig. 18. Space of possible index for 87.4% SL propellant with three nominal AP particle sizes – 400, 50, 20  $\mu\text{m}$  at 68.9 atm.

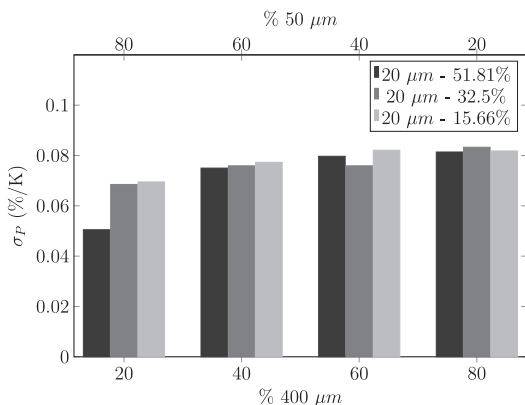


Fig. 19. Space of possible temperature sensitivity for 87.4% SL propellant with three nominal AP particle sizes – 400, 50, 20  $\mu\text{m}$  at 68.9 atm.

creased below 60%. Under such conditions a decrease in 20  $\mu\text{m}$  fraction leads to a decrease in index indicating the increased role of diffusion dominated burning of 50  $\mu\text{m}$  AP particle in controlling the burn rate variation with pressure. Temperature sensitivity variation with particle size distribution, as shown in Fig. 19, is consistent with the observations made earlier. It is lower than for AP at corresponding pressure and decreases with the decrease in the fraction of 400  $\mu\text{m}$  AP consistent with the increased role of binder with lower particle sizes. Similar variations were obtained with 84% AP with corresponding burn rates reduced by about 12% on average.

#### 4. Effect of burn rate modifiers

Burn rate modifiers can either be catalysts that enhance the burn rate or inhibitors. Iron oxide (IO), Copper Chromite (CC) and activated carbon (ACR) are the most common catalysts. Catalysts enhance the burn rate, predominantly by acting on the gas phase reaction between the decomposition products of HTPB and AP, since they are mixed with the binder during processing [36]. The fact that the pressure index is only marginally affected by addition of catalyst is indicative of the predominant gas phase effect. This can be accounted for in the current framework by suitably modifying the activation energy of the gas phase reaction. The extent to which the activation energy must be decreased, which will be a function of the catalyst concentration, can be estimated from the measured burn rate enhancement of fine AP/HTPB premixed propellant with increasing fraction of catalyst. Information on the saturation limit of catalysis can also be obtained from the same data.

Titanium dioxide ( $\text{TiO}_2$ ), Lithium fluoride (LiF) etc., are the common inhibitors. Recently Strontium carbonate ( $\text{SrCO}_3$ ) is being used as an inhibitor to achieve low pressure index ( $\leq 0.3$ ). Here we will focus on  $\text{SrCO}_3$  as it is the preferred inhibitor amongst the practitioners in India. While an approach similar to that used for catalysts can be used to account for the effect of inhibitors, by increasing the activation energy instead of decreasing it, that alone cannot explain the significant reduction in pressure index observed with addition of about 2–3%  $\text{SrCO}_3$ . Reduction in pressure index beyond the limit that can be explained by diffusion alone, which is  $\sim 0.4$ , is indicative of significant changes in the surface behavior with addition of inhibitors, especially,  $\text{SrCO}_3$ . An important point to note is that, when the pressure index is as low as 0.25, the burn rate of the propellant can drop below that of AP at pressures as low as 50 atm (LRSAM propellant in Fig. 1). This effect, indicating significant reduction in the flux received by the propellant surface compared to the base propellant (without the inhibitor), can be explained only by invoking binder melt coverage of AP surface.

Addition of a few %  $\text{SrCO}_3$  to AP/HTPB based composite propellants is known to bring down the burn rate dramatically (see [37]). It is also clear from the data presented in [37] that the catalytic effect saturates at 5%  $\text{SrCO}_3$ . Experimental results for composition C9P6 (see Table 2) also show similar reduction in burn rate along with reduction in pressure index to values less than 0.3. Based on these observations it is hypothesized that the  $\text{SrCO}_3$  reduces the burn rate by an interconnected mechanism of inhibition of gas phase reaction (between decomposition products of HTPB and AP) and binder melt flow over AP surfaces. As described earlier, in the framework of the current model, the inhibition of gas phase reaction is accounted for by an increase in activation energy ( $E_g$ ) and the magnitude of change in  $E_g$  can be estimated from the reduction in burn rate of premixed fine-AP/HTPB/ $\text{SrCO}_3$  propellants compared to the base propellant without  $\text{SrCO}_3$ . Reduction in the gas phase reaction rate decrease the heat flux received by the surface which will in turn lead to enthalpy deficit for decomposition of HTPB leading to flow of this melt over AP surface. In addition to this,  $\text{SrCO}_3$  itself can undergo endothermic decomposition at around 1100 K causing a jump in the temperature profile leading to further reduction in heat flux received by the surface. If  $\text{SrCO}_3$  decomposes endothermically with an enthalpy change of  $H_d$  (kJ/kg) at a non-dimensional distance,  $\xi_d = \rho_p \dot{r} c_p x_d / k$ , from the propellant surface, then the heat flux balance at the surface will take the form shown in Eq. (19).

$$\rho_p \dot{r} c_p (T_s - T_0) = \rho_p \dot{r} H_s + \frac{\rho_p \dot{r} c_p (T_d - T_s) f_{\text{mll}}}{e^{\xi_d} - 1} \quad (19)$$

$$\Rightarrow \xi_d = \ln(1 + B_{ds}) \quad (20)$$

where,  $T_d$  is the decomposition temperature of  $\text{SrCO}_3$  (taken as 1100 K),  $H_s$  is the enthalpy change at the surface due to AP and HTPB decomposition and  $B_{ds} = (T_d - T_s)/(T_s - T_0 - H_s/c_p)$ , the decomposition transfer number. The crucial difference between this equation compared to that for the case without  $\text{SrCO}_3$  is the replacement of the geometric factor ( $g_f$ ) with  $f_{nll}$ , which denotes the fraction of the AP surface not covered by binder melt. This factor, in addition to the geometric effect, will account for the additional coverage of the AP surface by binder melt. The factor,  $f_{nll}$  is related to the geometric factor ( $g_f$ ) as shown in Eq. (21).

$$f_{nll} = g_f - f_{ll} \quad (21)$$

where  $f_{ll}$  is the fraction of the AP surface covered by binder melt in addition to the geometric effect. An expression for this will be described later. A heat flux balance in the plane of decomposition ( $\xi_d$ ) is given by Eq. (22).

$$\left[ \frac{\rho_p \dot{r} c_p (T_f - T_d)}{e^{\xi_d} - e^{\xi_d^*}} \right] \xi_d = \left[ \frac{\rho_p \dot{r} c_p (T_d - T_s)}{e^{\xi_d} - 1} \right] \xi_d + \rho_p \dot{r} f_{SC} H_d \quad (22)$$

where,  $H_d$  is the decomposition enthalpy of  $\text{SrCO}_3$ , taken as 1300 kJ/kg (endothermic) corresponding to  $\text{SrO}$  and  $\text{CO}_2$  as final products and  $f_{SC}$ , the fraction of  $\text{SrCO}_3$  around each AP particle. Eqs. (19) and (22) along with the overall mass balance, given by  $\rho_p \dot{r} = K_r p^2 x^*$  is solved iteratively to get  $\xi_d^*$  and  $\xi_d$ . With increase in pressure, the limit,  $T_s \rightarrow T_d$  will be approached; this corresponds to decomposition at the surface. In this limit,  $\xi_d = 0$  and the enthalpy of decomposition of  $\text{SrCO}_3$  is accounted for in the  $H_s$  term.

#### 4.1. Binder melt effect

The binder melt effect is similar to the 'blocking effect' well known in the hybrid rocket literature [38]. It refers to the shielding of heat flux received by the fuel surface due to high molecular weight fragments generated by the decomposition of the polymer. The binder melt in composite propellants represents an extreme version of this shielding where the heat feedback is blocked to an extent that it is insufficient to vaporize the HTPB. While in uncatalyzed propellants this effect might start to play a role when the overall SL drops to very fuel rich conditions, the presence of  $\text{SrCO}_3$  along with the binder shifts the limit to high SL. Drawing from the hybrid rocket regression relationship [38], the fraction of the AP surface covered by binder melt ( $f_{ll}$ ) is expressed as a function of the decomposition transfer number ( $B_{ds}$ ) as shown in Eq. (23).

$$f_{ll} = C f_{SC} (a + B_{ds})^{-2} \quad (23)$$

where  $f_{ll}$  is the surface covered by liquid layer in addition to the geometric factor,  $f_{SC}$  is the fraction of  $\text{SrCO}_3$  in a binder-matrix coated AP particle,  $a$  is a positive constant to ensure that the value of  $f_{ll}$  remains bounded as the pressure increases since  $B_{ds}$  decreases with pressure. The negative exponent on  $B_{ds}$  accounts for the increase in binder melt cover with pressure. At this stage, the model is calibrated using the experimental results of C9P6 (see Fig. 20);  $C$  is taken as 6.5 and that of  $a$  as 0.35. A 10% change in  $c$  and  $a$  leads to less than 5% change in the burn rates and hence the results are not found to be sensitive to the choice of values for  $C$  and  $a$ . Predictions for other values of fraction of  $\text{SrCO}_3$  maintaining the same coarse to fine ratio as C9P6 is shown in Fig. 20 along with the result with 0%  $\text{SrCO}_3$ . This approach needs more experimental data on fine AP based propellants without and with additives, it appears that the essential features of the effects are captured by this formalism. Some preliminary work with a developmental laboratory showed that the burn rate behavior was well captured by the base propellant even when the experimental data was consciously brought in later. More work in this direction is currently planned.

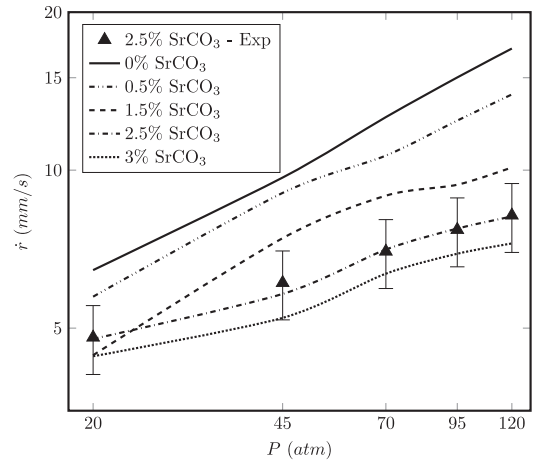


Fig. 20. Predicted effect of  $\text{SrCO}_3$  on the burn rate of AP/HTPB propellants with fixed coarse to fine ratio.

## 5. Conclusions and future work

A novel framework based on the 'Heterogeneous quasi-1D model' combined with a serial burning geometric description has been presented for understanding the influence of AP particle size distribution on the burn rate of composite solid propellants. Identification of pure AP and premixed AP/HTPB propellants as the canonical flames for estimating model parameters is the most important outcome of this work. A total of 50 propellants, covering a wide range of solid loading and particle size distributions, taken from literature was analyzed using this framework. AP particles smaller than the pressure dependent premixed cut-off limit were homogenized with HTPB and was used to determine the *critical pressure*, the pressure beyond which the binder-matrix can undergo self-sustained deflagration. Based on the critical pressure, the 50 propellants were classified into two groups – 26 conventional and 24 HFF propellants and further analysis was focused on conventional propellants as they are the most widely used practical propellants. Accounting for the detailed particle size distribution brought out the wide variation in O/F of particles constituting a propellant, something not attempted by earlier modeling work, has been shown to be crucial to better predictions of burn rates and in uncovering of the phenomenon of *local extinction* – quenching of fuel rich particles due to surface temperature, determined from the heat balance, dropping below the LPDL of AP (870 K). The excellent predictive capability of the model, partly due to accounting for local extinction, is demonstrated by comparison of calculated burn rates for all conventional propellants (26 nos.) with experimental results from earlier literature. Hitherto unexplored quantitative relation between the temperature sensitivity of propellants and AP is used to establish that the temperature sensitivity of an AP based composite propellant will always be less than that of the AP used in the formulation – which itself can vary widely due to contaminants. This feature is suggestive of an approach to reduce temperature sensitivity of propellants remaining unaddressed till now. The framework is extended to account for the influence of burn rate modifiers and a particularly difficult case arising out of addition of the burn rate suppressing agent, strontium carbonate ( $\text{SrCO}_3$ ), is analyzed. Parameters calibrated to capture the burn rate variation of propellant C9P6 (2.5%  $\text{SrCO}_3$ ) are used to obtain predictions with varying quantities of  $\text{SrCO}_3$ , which can be used as candidate propellants for further experimental studies and validation of the liquid layer model proposed here.

## References

- [1] N.S. Cohen, Review of composite propellant burn rate modeling, *AIAA J.* 18 (3) (1980) 277–293.
- [2] M.W. Beckstead, R.L. Derr, C.F. Price, The combustion of solid monopropellants and composite propellants, *Symp. (Int.) Combust.* 13 (1971) 1047–1056, doi:10.1016/S0082-0784(71)80103-0.
- [3] R.L. Glick, On statistical analysis of composite solid propellant combustion, *AIAA J.* 12 (3) (1974) 384–385.
- [4] N.S. Cohen, L. Strand, An improved model for the combustion of ap composite propellants, *AIAA J.* 20 (12) (1982) 1739–1746.
- [5] F. Blomshield, Nitramine composite solid propellant modelling (Final Report, December 1984–December 1988), Technical Report NWC TP 6992, Naval Weapons Center, 1989.
- [6] R.R. Miller, Effects of particle size on reduced smoke propellant ballistics, *AIAA paper* 1096 (1982).
- [7] G. Knott, T. Jackson, J. Buckmaster, Random packing of heterogeneous propellants, *AIAA J.* 39 (4) (2001) 678–686.
- [8] S. Kochevets, J. Buckmaster, T. Jackson, A. Hegab, Random packs and their use in modeling heterogeneous solid propellant combustion, *J. Propuls. Power* 17 (4) (2001) 883–891.
- [9] L. Massa, T. Jackson, J. Buckmaster, New kinetics for a model of heterogeneous propellant combustion, *J. Propuls. Power* 21 (5) (2005) 914–924.
- [10] L. Massa, T. Jackson, J. Buckmaster, M. Campbell, Three-dimensional heterogeneous propellant combustion, *Proc. Combust. Inst.* 29 (2) (2002) 2975–2983.
- [11] T.L. Jackson, Modeling of heterogeneous propellant combustion: a survey, *AIAA J.* 50 (5) (2012) 993–1006.
- [12] M.L. Gross, T.D. Hedman, S.F. Son, T.L. Jackson, M.W. Beckstead, Coupling micro and meso-scale combustion models of ap/htpb propellants, *Combust. Flame* 160 (5) (2013) 982–992.
- [13] M.L. Gross, Towards a predictive propellant burning rate model based on high-fidelity numerical calculations, 46th AIAA/ASME/SAE/ASEE Joint Propulsion Conference & Exhibit (2010), p. 6914.
- [14] P.A. Ramakrishna, P.J. Paul, H.S. Mukunda, Sandwich propellant combustion: modeling and experimental comparison, *Proc. Combust. Inst.* 29 (2) (2002) 2963–2973.
- [15] P.A. Ramakrishna, Sandwich propellant combustion – computational studies and experimental comparisons, Indian Institute of Science, Bangalore, 2003 (Ph.D. thesis).
- [16] G. Lengelle, J. Duterque, J. Trubert, Physico-chemical mechanisms of solid propellant combustion, solid propellant chemistry, combustion, and motor interior ballistics (A 00–36332 09–28), *Progress in Astronautics and Aeronautics*, 185, American Institute of Aeronautics and Astronautics, Inc., Reston, VA, 2000, pp. 287–334.
- [17] T.L. Boggs, D.E. Zurn, The temperature sensitivity of the deflagration rates of pure and doped ammonium perchlorate, *Combust. Sci. Technol.* 4 (1) (1971) 227–232.
- [18] S. Varunkumar, H.S. Mukunda, Progress report on solid rocket combustion instability modelling, Technical Report IITRPR-SMMEE-2013-001, IISc & IIT Ropar, 2013.
- [19] M. Beckstead, A model for solid propellant combustion, *Symp. (Int.) Combust.* vol. 18 (1981) 175–185.
- [20] A.R. Kerstein, Percolation model of polydisperse composite solid propellant combustion, *Combust. Flame* 69 (1) (1987) 95–112.
- [21] R.A. Fredrick Jr, Combustion mechanisms of wide distribution propellants, Technical Report AFAL-TR-88-008, DTIC Document, 1988.
- [22] A. Iyer, N.R. Balamurali, S. Varunkumar, Random packing of multi-modal spheres in a cubic box a model for understanding AP/HTPB based composite solid propellants, International Autumn Seminar on Propellants, Explosives and Pyrotechnics, Qingdao, 2015 (2015).
- [23] E.W. Price, Effect of multidimensional flamelets in composite propellant combustion, *J. Propuls. Power* 11 (4) (1995) 717–729.
- [24] N.S. Cohen, R.W. Fleming, R. Derr, Role of binders in solid propellant combustion, *AIAA J.* 12 (2) (1974) 212–218.
- [25] D.M. Hanson-Parr, T.P. Parr, Thermal properties measurements of solid rocket propellant oxidizers and binder materials as a function of temperature, *J. Energetic Mater.* 17 (1) (1999) 1–48.
- [26] M.L. Gross, M.W. Beckstead, Diffusion flame calculations for composite propellants predicting particle-size effects, *Combust. Flame* 157 (2010) 864–873, doi:10.1016/j.combustflame.2009.09.004.
- [27] R. Foster, J. Condon, R. Miller, Low exponent technology, US Air Force Rocket Propulsion Lab., 1982. TR-82-060, Edwards AFB, CA
- [28] N. Kubota, Propellants and explosives, John Wiley & Sons, 2007.
- [29] I. Kumar, P.A. Ramakrishna, Enhancing composite solid propellant burning rates with potassiumdoped ammonium perchlorate – part – 2, *J. Propuls. Power* 30 (4) (2014) 876–882.
- [30] F. McIntyre, Hazards testing of ammonium perchlorate, Technical Report ARL-CD-CR-82026, DTIC Document, 1982.
- [31] M. Brewster, The effect of propellant optical properties on composite solid propellant combustion, Technical Report N00014-87-0547, DTIC Document, 1991.
- [32] F. Blomshield, J. Osborn, Nitramine composite solid propellant modeling, Joint Propulsion Conferences, American Institute of Aeronautics and Astronautics (1990).
- [33] K. Ishitha, P. Ramakrishna, Studies on the role of iron oxide and copper chromite in solid propellant combustion, *Combust. Flame* 161 (10) (2014) 2717–2728.
- [34] T.L. Boggs, E.W. Price, D.E. Zurn, The deflagration of pure and isomorphously doped ammonium perchlorate, *Symp. (Int.) Combust.* vol. 13 (1971) 995–1008.
- [35] N.S. Cohen, D.A. Flanigan, Mechanisms and models of solid-propellant burn rate temperature sensitivity—a review, *AIAA J.* 23 (10) (1985) 1538–1547.
- [36] J.C. Handley, An experimental investigation of catalysis in the combustion of composite solid propellants, Georgia Institute of Technology, 1976 (Ph.D. thesis).
- [37] J. Craig, Solid propellant containing strontium carbonate-calcium citrate burning rate depressant, 1974, US Patent 3,841,929.
- [38] P. Paul, H. Mukunda, V. Jain, Regression rates in boundary layer combustion, *Symp. (Int.) Combust.* vol. 19 (1982) 717–729.